Dynamics of electron-trapping materials under blue light and near-infrared exposure: an improved model

Ramin Pashaie[1,*] and Nabil H. Farhat[1,2]

[1]*Department of Electrical and System Engineering, University of Pennsylvania, 200 South 33rd Street, Philadelphia, Pennsylvania 19104-6391, USA*

[2]*Institute of Neurological Sciences, University of Pennsylvania, 3450 Hamilton Walk, Philadelphia, Pennsylvania 19104-6074, USA*

[*]*Corresponding author: raminp@seas.upenn.edu*

Received January 8, 2007; accepted April 10, 2007;
posted April 26, 2007 (Doc. ID 78556); published xx xx, xxxx

Dynamics of electron-trapping materials (ETMs) is investigated. Based on experimental observations, evolution of the ETM's luminescence is mathematically modeled by a nonlinear differential equation. This improved model can predict dynamics of ETM under blue light and near-infrared (NIR) exposures during charging, discharging, simultaneous illumination, and in the equilibrium state. The equilibrium-state luminescence of ETM is used to realize a highly nonlinear optical device with potential applications in nonlinear optical signal processing. © 2007 Optical Society of America

OCIS codes: 160.2540, 200.4560, 200.3050.

1. INTRODUCTION

Electron-trapping materials (ETMs) are alkaline-earth sulfides doped with rare-earth luminescence centers [1,2]. Such a material possesses versatile optical properties, including high resolution and wavelength diversity, which make it attractive for a variety of technical applications [1,2]. ETM has been employed in the structure of computational machines such as parallel Boolean logic [3], spatial domain match filtering [4], associative memory [5–7], and adaptive learning [8], as well as optical data storage [1,2], infrared sensors, image intensifiers, and medium-wavelength infrared to visible converters [9,10].

The atomic structure and the dynamics of ETM under blue light and near-infrared (NIR) illumination have been known for sometime [11], and a few approximate models for the optical mechanism of ETM have been presented [12,13]. The first-order mathematical model that governs the ETM's dynamics was proposed in 1993 [12]. This model contained several restrictions; namely, it assumed the trapped electron density is far from saturation, and the effect of interaction between blue photons and the trapped electrons is negligible. Furthermore, in this model, electron-trapping efficiency was assumed to be independent of the current level of the trapped electron density. With these simplifications, the charging and discharging processes were modeled by linear and exponential functions, respectively.

A modified version of this early model was presented in 1995 [13] that took into account some of the previously neglected effects. In this modified model, the intensity of the ETM's luminescence was a function of the intensity of both the charging blue light and the discharging NIR exposures. Also, the saturation in the density of trapped electrons was considered in the equations. Both charging and discharging processes were exponential. Nevertheless, predictions of the model do not agree well with experimental results.

Extending the utility of ETMs to quantitative applications requires a mathematical model that predicts its unique dynamics precisely. In this paper, we present an improved model that can simulate the evolution of ETM's luminescence during charging and discharging, including simultaneous blue light and NIR exposure, and in the equilibrium state. Predictions of the model agree with experimental observations.

In Section 2 we briefly review the physics and the optical mechanism of ETM. The chain of experiments that led us to the improved model are detailed in Section 3, and the mathematical model is presented in Section 4. Section 5 is devoted to the equilibrium-state luminescence of ETM. We show how the equilibrium state of an ETM can be used to conceive nonlinear optical devices. Concluding remarks are given in Section 6.

2. DYNAMICS OF ETM UNDER BLUE LIGHT AND NEAR-INFRARED ILLUMINATION

The ETM used in this study is $SrS:Eu^{2+},Sm^{3+}$, which is basically wide-bandgap strontium sulfides (SrS) doped with two types of selected rare-earth elements, Eu^{2+} and Sm^{3+}. Fabrication of relatively large-area thin films of this ETM is easy. The atomic structure and the optical mechanism of ETM under simultaneous blue light and NIR exposure are depicted in Fig. 1. Both of the two rare-earth doping elements have ground and excited states within the wide bandgap of the host; however, the luminescence centers of Eu^{2+} can easily give up an electron to become Eu^{3+}, and the electron-trapping centers of the

0740-3224/07/080001-0/$15.00

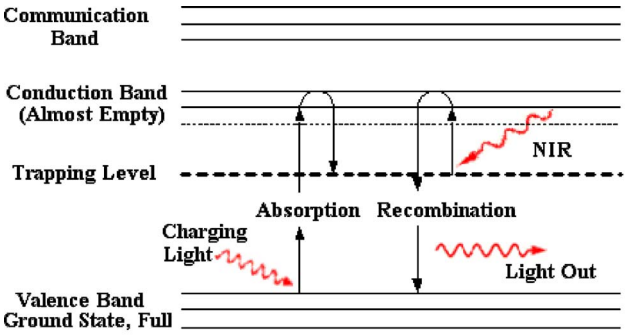

Color: Online

Fig. 1. (Color online) Optical mechanism of charging and discharging of ETM. Interaction of blue photons and electrons of the valence band excites the electrons and sends them to the communication band. Those excited electrons will tunnel to the trap level and become trapped electrons. Infrared photons give sufficient energy to the trapped electrons to detrap and excite them to the communication energy level. These electrons release their extra energy in the form of orange luminescence during their return to the valence band.

Sm^{3+} can easily accept an electron to become Sm^{2+}. Absorption of blue light with a peak response at ≈450 nm excites electrons from the ground state to the excited state of Eu^{2+} ions. Once in the excited state, electrons tunnel to neighboring Sm^{3+} sites and then fall to the ground state to become trapped electrons, leaving behind Eu^{3+} and Sm^{2+} ions.

Blue photons can also provide sufficient energy to kick the electrons from the trap level to the communication level, where they may interact and return to the ground state accompanied by the emission of photons with peak response at ≈640 nm (orange light luminescence). However, when the density of trapped electrons is much lower than the density of electrons in the valence band, the probability of interaction between blue photons and electrons of the valence band is higher than having such an interaction with trapped electrons. If blue light illumination persists for a while, a greater number of electrons will be trapped, which increases their chance of interacting with blue photons. As a result, if an ETM with empty trap levels is exposed to blue light illumination, the intensity of the orange light emission will reach the saturation level after a sharp growth. The intensity of orange light emission during blue light exposure can be used as a means of estimating the density of trapped electrons.

When the blue light is removed, the information carried in by the blue light pattern is stored in the ETM as a trapped electron density distribution. If the charged ETM is exposed to uniform NIR light with peak response at ≈1310 nm, sufficient energy is provided that the trapped electrons are excited from the ground state of Sm^{2+} to the excited state and tunnel back to neighboring Eu^{3+} sites. Again, subsequent relaxation from the Eu^{3+} excited state to the ground state produces emission of orange light. Under simultaneous illumination of the ETM by constant blue light and NIR exposure, after a transient response, orange emission converges to a constant value that is the equilibrium-state luminescence of the ETM.

Since the mechanism involved is purely electronic, ETMs are fast, possessing nanosecond response times under both blue light and infrared illuminations. They provide long-term storage of information when kept dark and have potential for high-density storage (>100 lp/mm) when fabricated in crystalline thin film form [14].

AQ: #2

3. EXPERIMENTS

An ordered sequence of experiments has been carried out to verify the dynamics of ETM with the experimental setup illustrated in Fig. 2. A thin layer of electron-trapping material deposited on a 25 mm × 25 mm layer of quartz [15] is exposed to two different sources of light: a bright blue LED and an Exalos 20 mW fiber coupled 1310 nm NIR superluminescence laser diode. A center-hole dark mask is placed on the ETM panel. This mask defines the area of the ETM under illumination in the following experiments. A blue optical filter blocks possible infrared radiation of the blue LED. Drivers of both light sources are precisely controlled by digital-to-analog converters (DACs) of a microcontroller board. An orange optical filter (Semrock LP01-633Rs-25) is placed in front of a cooled avalanche photodiode (APD) module (Hamamatsu CA4777-01) to measure the orange luminescence of the ETM.

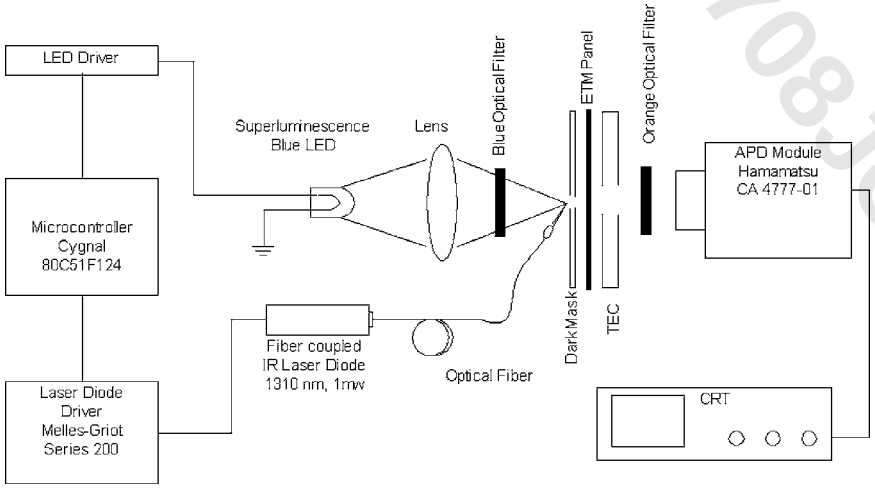

Fig. 2. Schematic of the experimental setup used for investigation of the ETM's dynamics.

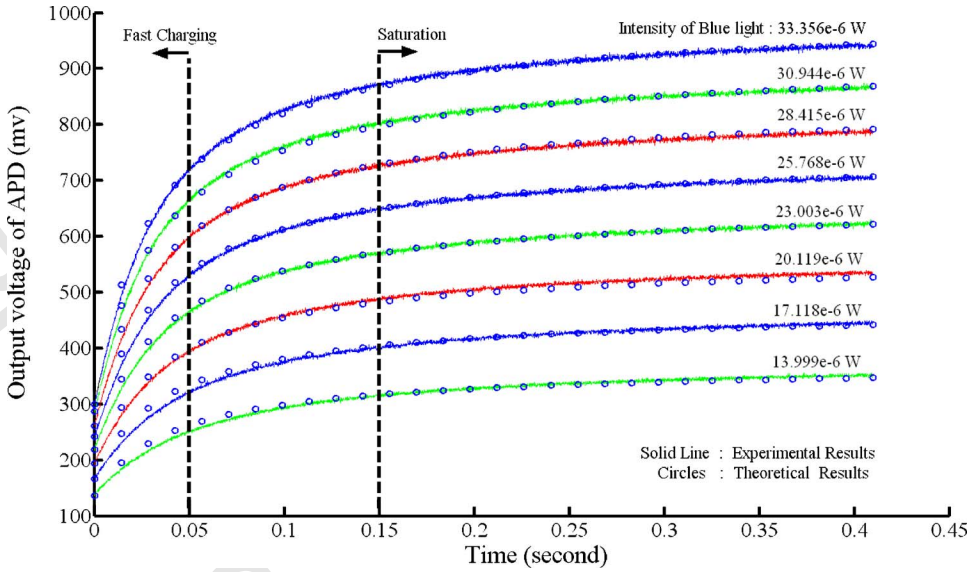

Color: Online

Fig. 3. (Color online) Charging characteristic curves of the partially erased ETM under blue light illumination. Three points should be considered in the study of these curves: the initial jumps (at $t=0.0$), the relatively linear buildup in the initial moments, and the final saturations. The solid curves are the experimental results, and the circles are the curve-fitting data.

The output voltage of the APD module is connected to the analog input terminal of the microcontroller's analog-to-digital converter (ADC). A center-hole thermoelectric cooler (TEC) is thermally coupled to the quartz substrate. Cooling the ETM decreases the chance of electron-phonon interaction and the self-luminescence of the phosphor. Also, it has been shown that the orange light emission of the ETM increases by decreasing the temperature of the material [16]. Therefore, the TEC improves the signal-to-noise ratio.

In the first experiment, we investigate the charging process of the ETM under blue light illumination. At the beginning, the blue LED is off when the ETM is exposed to the NIR laser, and the APD module measures the intensity of the orange light emission. When the output voltage of the APD reaches a constant predefined value, the microcontroller's DAC turns off the NIR laser and turns on the blue LED with a specified electric current. Next, the microcontroller's ADC digitizes and records the output voltage of the APD for a fraction of a second.

We repeat a similar protocol sequentially with different blue light intensities. Figure 3 displays the charging characteristic curves developed. Three key points should be noted in the study of the results obtained: the initial jump in the intensity of the emitted orange light at the beginning of the blue light illumination, its relatively linear behavior during the initial few milliseconds, and the final saturation.

The existence of different saturation levels can be justified by considering that blue photons have sufficient energy not only to excite the electrons of the valence band and send them to the trap level, but also to detrap some of the trapped electrons. The final saturation represents the equilibrium state of these two opposing processes. The

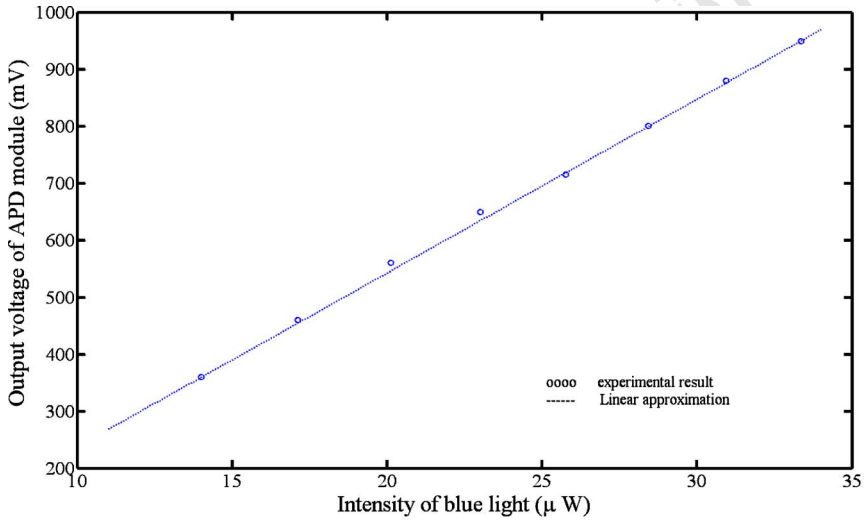

Color: Online

Fig. 4. (Color online) Saturation levels of the partially erased ETM as a function of the charging blue light intensity and the corresponding linear approximation.

level of saturation is a function of the blue light intensity. This dependency can be approximated by a linear function as shown in Fig. 4. Although the ETM is primarily erased to the same density of trapped electrons before all the charging periods, each curve has a different initial jump. This observation suggests that under blue light illumination the intensity of orange light luminescence is a function of both the trapped-electron density and the intensity of the incident blue light.

The saturation level of the orange light emission is one of the ETM's critical parameters in the design of nonlinear optical devices (as will be described later) and it needs to be investigated further. From the charging curves of Fig. 3, it is apparent that the saturation level is a function of the blue light intensity. However, these curves were developed by charging an ETM that was primarily discharged to a constant predefined trapped-electron density. Hence, an unanswered question remains: Does the intensity of orange luminescence reach the same saturation level when the charging process, with constant blue light intensity, starts from different trapped-electron densities?

To answer this question, a series of experiments was performed as follows. First, the precharged ETM is exposed to an intense NIR light while the APD module measures the level of the orange light emission. Next, for a fraction of a second, the partially discharged ETM is illuminated by a constant blue light. Simultaneously, the microcontroller's ADC digitizes and records the intensity of the orange light luminescence. We repeat this experiment with a similar protocol, but in each trial, the NIR light is turned off at different values of the APD output voltage. Thus, the charging process in each trial starts from a different density of trapped electrons. The curves developed in this process are displayed in Fig. 5. The curves of Fig. 5(b) are similar to the ones illustrated in Fig. 5(a) with more emphasis on initial moments. The experimental results in Fig. 5(a) show that the final saturation level is independent of the initial trapped-electron density. The curves of Fig. 5(b) illustrate that the slope of the charging curve depends on the initial conditions. The charging curves that start from a higher density of the trapped electrons have larger slopes compared with the curves

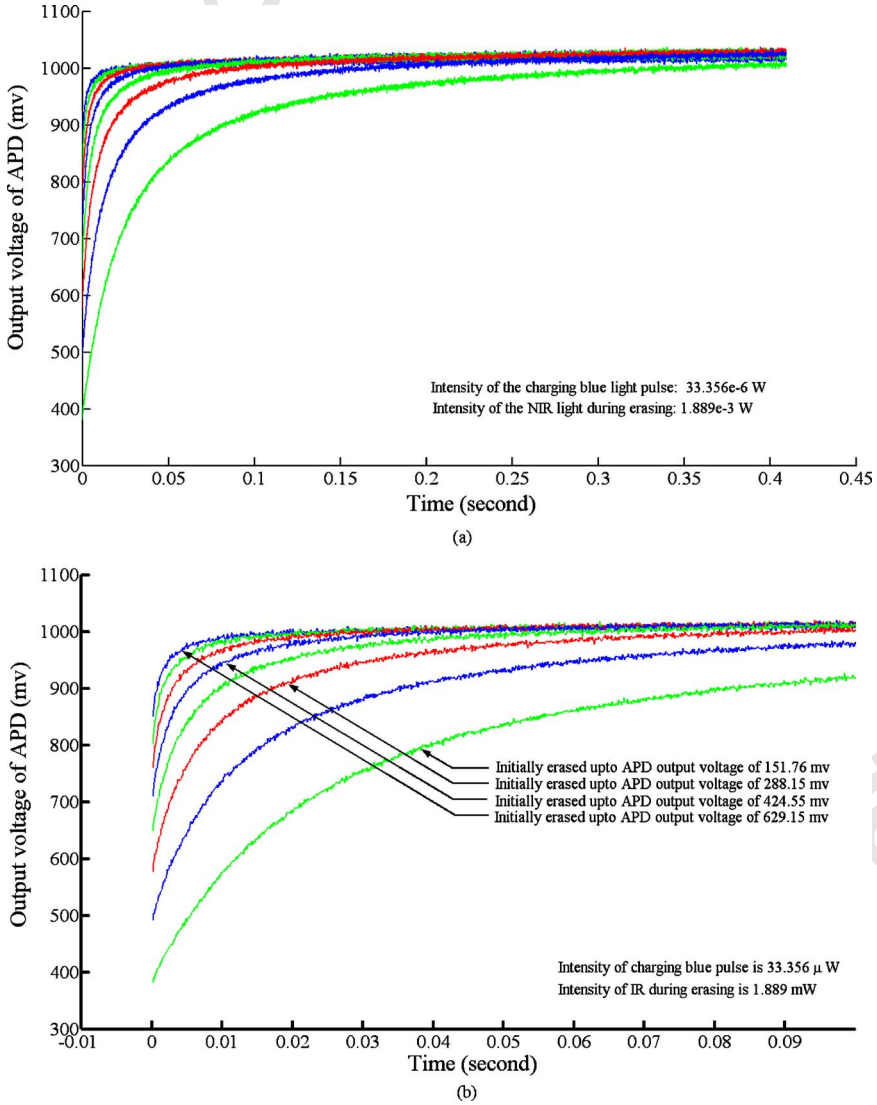

Color: Online

Fig. 5. (Color online) Charging of the partially erased ETM by constant blue light illumination. (a) Despite different initial density of trapped electrons, all the curves merge to the same saturation level. (b) Different initial jumps under constant blue light illumination.

starting from a lower trapped-electron density. The ETM charges faster when the charging process starts with a higher density of trapped electrons. This observation will be used later in the design of a nonlinear optical device.

Figure 6(a) displays the levels of the initial jumps as a function of the intensity of the blue light when the initial density of the trapped electrons is constant. It is clear that the experimental data can be approximated by a linear function. The graph of Fig. 6(b) illustrates the levels of the initial jumps as a function of the initial trapped-electron density, when the intensity of the incident charging blue light is constant. Again, the experimental data developed can be approximated by a linear function. By investigating the data developed from these experiments, the relation between the intensity of the orange luminescence and the intensity of the charging blue light can be formulated. The intensity of the orange light emission is a linear function of the blue light intensity when the charging process starts from equal initial densities of trapped electrons. The intensity of the orange luminescence is also a linear function of the density of the trapped electrons during the charging process with constant blue light intensity. Consequently, the intensity of the orange light emission during the charging process is proportional to the product of the current value of the trapped-electron density and the intensity of the blue light.

The same experimental setup is used to extract the discharging curves of ETM. We perform this experiment in three sequential steps. First, the ETM is exposed to intense NIR illumination that detraps almost all the trapped electrons. In the second step, the ETM is exposed to a pulse of blue light with a constant intensity and duration. In the third and last step, the ETM panel is illuminated by a constant NIR light while the intensity of the emitted orange light is digitized and recorded. Then, the same protocol is repeated by changing the intensity of the NIR light in the last step of the experiment. The group of curves displayed in Fig. 7 represents the results of the

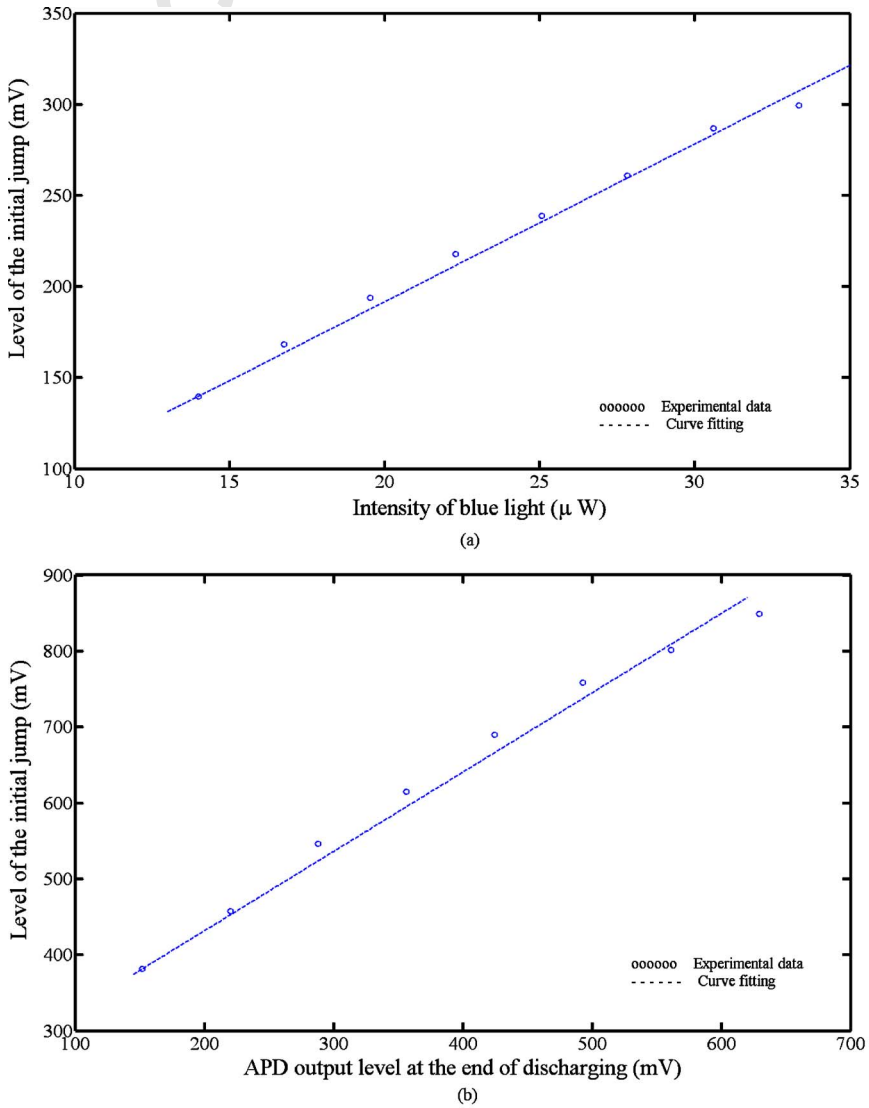

Color: Online

Fig. 6. (Color online) (a) Levels of the initial jumps as a function of the intensity of the blue light when the initial density of the trapped electrons is constant. The experimental data can be approximated by a linear function. (b) The levels of the initial jumps as a function of the initial trapped-electron density when the intensity of the incident charging blue light is constant. Again, the experimental data can be approximated by a linear function.

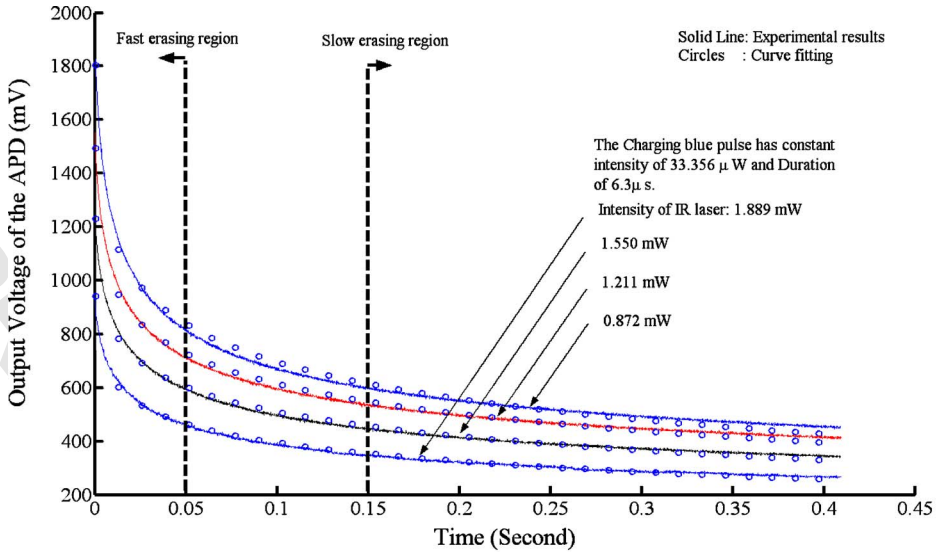

Color: Online

Fig. 7. (Color online) Discharging characteristic curves of the ETM. The discharging process has two separable phases. In the first phase, the intensity of the orange light emission drops rapidly after an abrupt jump. During the second phase, the intensity of the orange light emission decreases slowly.

discharging experiment. These curves show that the discharging process has two different phases. During the first phase, which occurs at the initial moment, the intensity of the emitted orange light drops rapidly and the discharging process is even faster than the exponential function. The initial jumps and the slopes of the curves in this figure are functions of the initial density of the trapped electrons and the intensity of the NIR exposure, the higher the initial density of trapped electrons, the steeper the discharging process. During the second phase, the orange light emission decreases slowly and the discharging process is slow. Figure 8 displays the levels of the initial jumps as a function of the discharging NIR light intensity. The experimental results in this graph can be approximated by a linear function. Hence, as with the charging process, the intensity of the orange light emission during discharging is proportional to the product of the intensity of the NIR light and the existing value of the trapped-electron density.

Figure 9 illustrates the effect of temperature on the intensity of the orange light emission. In this experiment, the ETM panel is simultaneously exposed to the blue light and the NIR laser, and the equilibrium-state emission of the ETM is recorded under different TEC currents. This experiment elucidates that increasing the current of the TEC (which is equivalent to reducing the temperature of ETM) increases the intensity of the emitted orange light and improves the corresponding signal-to-noise ratio of the APD module output voltage. In practice, by cooling the ETM, detectors with lower sensitivity that are cheaper and available in array formats can be employed. This could become a critical issue during realization of multipixel systems. The temperature dependence of the photoluminescence in the singly doped ETMs ($SrS:Em^{2+}$

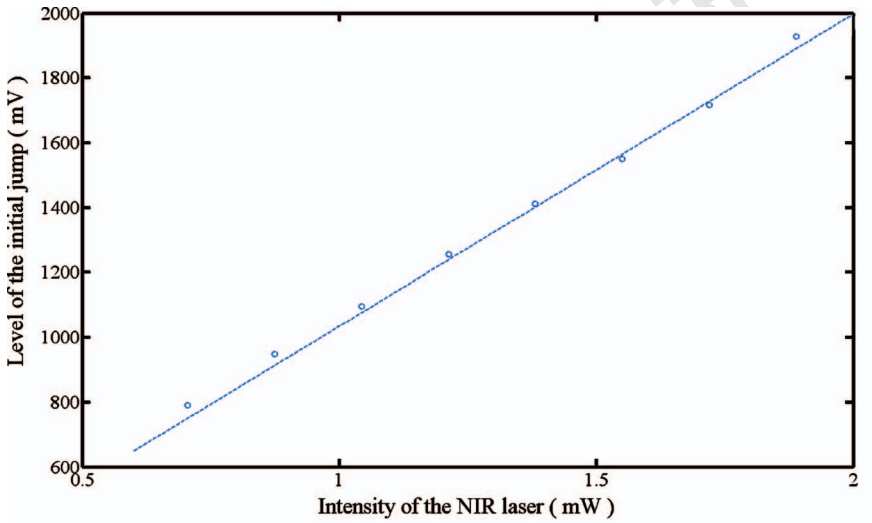

Color: Print

Fig. 8. Levels of the initial jumps as a function of the discharging NIR light intensity. A linear function can be fitted to the experimental results.

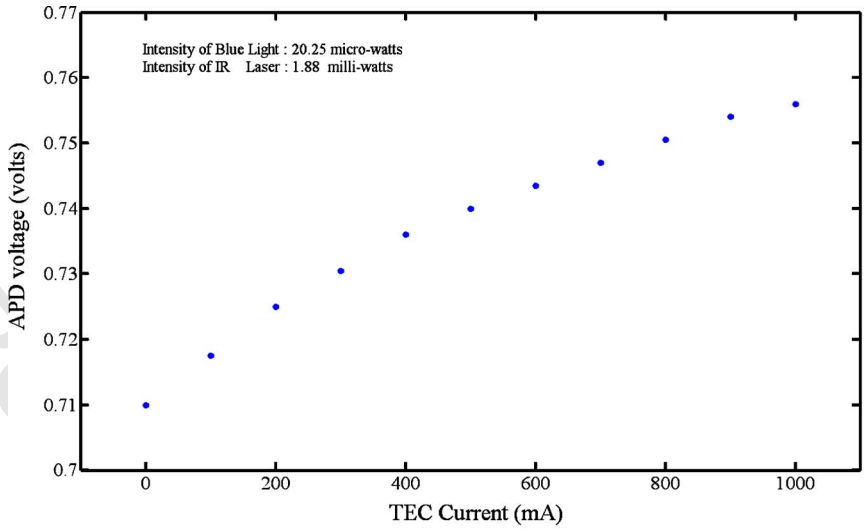

Color: Online

Fig. 9. (Color online) Effect of temperature on the intensity of the emitted orange light when the ETM is under simultaneous blue light and NIR light illumination. This curve proves that at lower temperatures, the orange light emission is more intense.

and SrS:Sm^{3+}) as well as the doubly doped ones (e.g. SrS:Em^{2+},Sm^{3+}) have been extensively studied [16].

4. MATHEMATICAL MODEL

In this section, the dynamics of the ETM under simultaneous blue light and NIR light illumination is cast in the form of a nonlinear differential equation based on the experimental results discussed in Section 3.

Suppose that $n(t)$ represents the temporal density of the trapped electrons as a function of time t. During the charging period when ETM is exposed just to the blue light, the density of the trapped electrons $n(t)$ increases monotonically from the initial density of the trapped electrons $n(0)$ to the saturation density n_s where $0 \leqslant n(t) \leqslant n_s$. By optimal curve fitting [17], the charging process can be formulated as

$$n(t) = n_s(I_B) - \xi I_B Ln\left(\frac{\eta}{t+t_s} + 1\right). \quad (1)$$

The saturation density of the trapped electrons is a function of the intensity of the incident blue light I_B. Following our experimental results (Fig. 4), the dependency of the n_s on the intensity of the charging blue light can be approximated by a linear function such as $n_s(I_B) = \kappa I_B$ where κ is a real constant.

During the discharging period when ETM is exposed to the NIR light, the density of the trapped electrons mono-

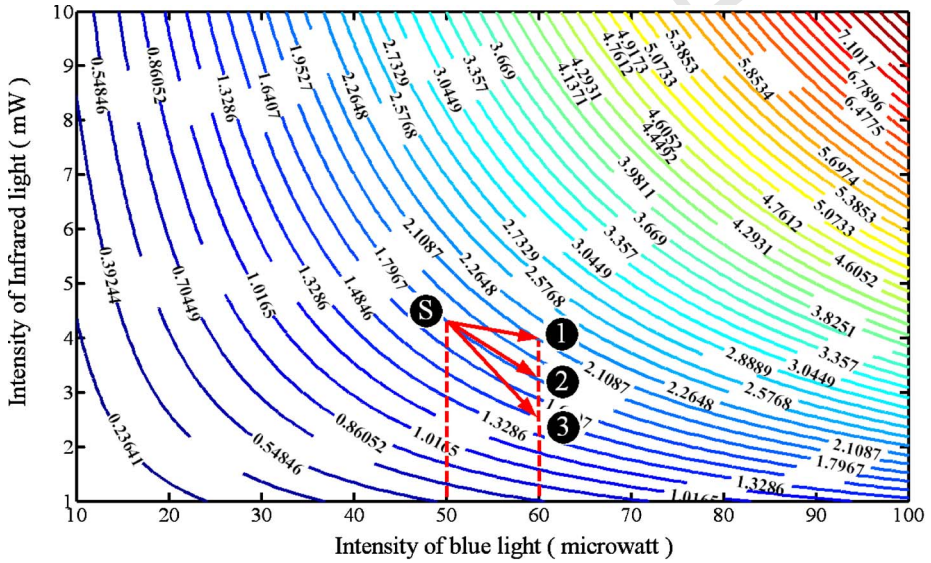

AQ: #7

Fig. 10. (Color online) ESP of electron-trapping material and the unexpected behavior of the ETM luminescence in the equilibrium state.

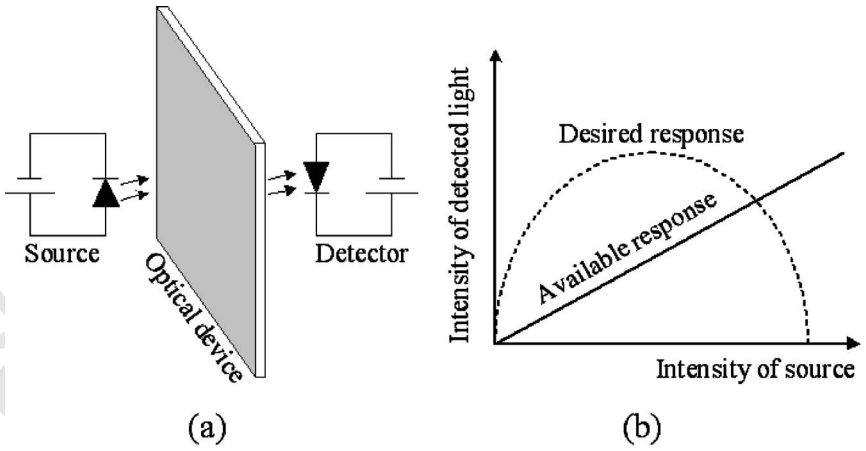

Fig. 11. (a) Optical setup. A light source illuminates the optical device and a detector measures the intensity of the light that passes through the optical device. (b) Available and desired response curves.

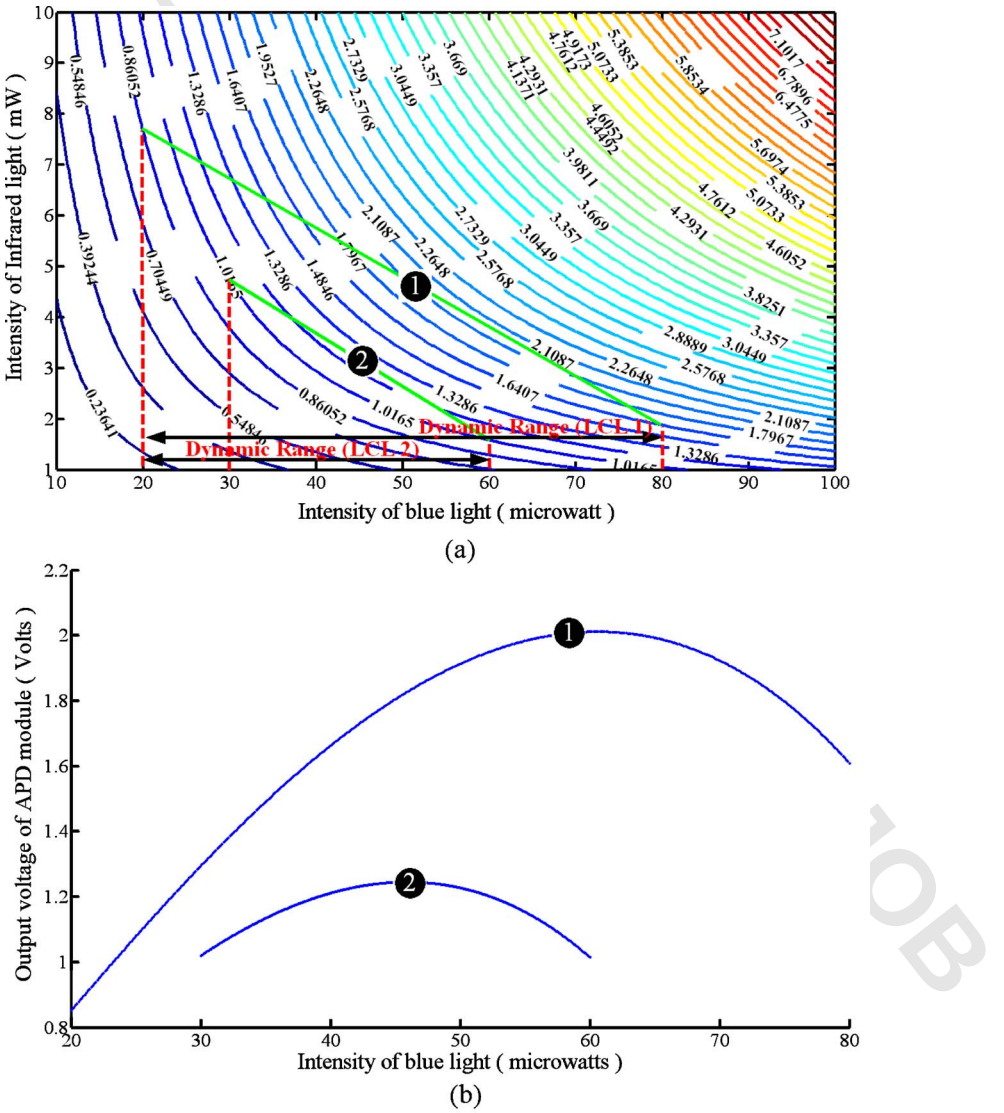

Color Online: Fig. 12. (Color online) (a) Two sample LCL and their dynamic ranges along the blue light intensity axis in the ESP of the ETM. Only the intensities of the emitted orange light along the LCLs are accessible when the light sources are linearly coupled. (b) The corresponding nonlinear curves.

tonically decreases. As with the charging process, the discharging process is formulated by optimal curve fitting [17] as

$$n(t) = \xi' I_{\mathrm{NIR}} Ln\left(\frac{\eta'}{t + t_{s'}} + 1\right) \tag{2}$$

where I_{NIR} is the intensity of the NIR light. In Eqs. (1) and (2), ξ and ξ' are the ETM wavelength-dependent sensitivity coefficients to the blue light and the NIR light exposures. Variables η and η' are the curve fitting parameters, and the initial jumps during the charging and the discharging processes are modeled by the variables t_s and $t_{s'}$, respectively. Obviously, t_s and $t_{s'}$ are functions of the initial density of the trapped electrons $n(0)$ and the intensity of the blue light and NIR exposure. The curve fittings of the experimentally derived data during charging and discharging processes are displayed in Figs. 3 and 7.

In Section 3 it was experimentally proved that I_{O}, the intensity of the orange light emission under simultaneous blue light and NIR illumination, can be expressed as

$$I_{\mathrm{O}}(t) = \alpha n(t) I_{\mathrm{B}} + \beta n(t) I_{\mathrm{NIR}} \tag{3}$$

where α and β are the proportionality coefficients for the blue light and the NIR light intensities. Usually, we measure the intensity of the orange luminescence by a photodetector. The output voltage of this transducer V_{O} is proportional to the illuminating optical intensity: $V_{\mathrm{O}} \propto I_{\mathrm{O}}$. From Eq. (1), the growth rate of the trapped-electron density is

$$\dot{n} = \frac{\mathrm{d}n}{\mathrm{d}t} = \frac{\xi I_{\mathrm{B}}}{\eta} \frac{\left[\exp\left(\frac{n_s - n}{\xi I_{\mathrm{B}}}\right) - 1\right]^2}{\exp\left(\frac{n_s - n}{\xi I_{\mathrm{B}}}\right)}. \tag{4}$$

Equation (1) can also be rearranged in the form

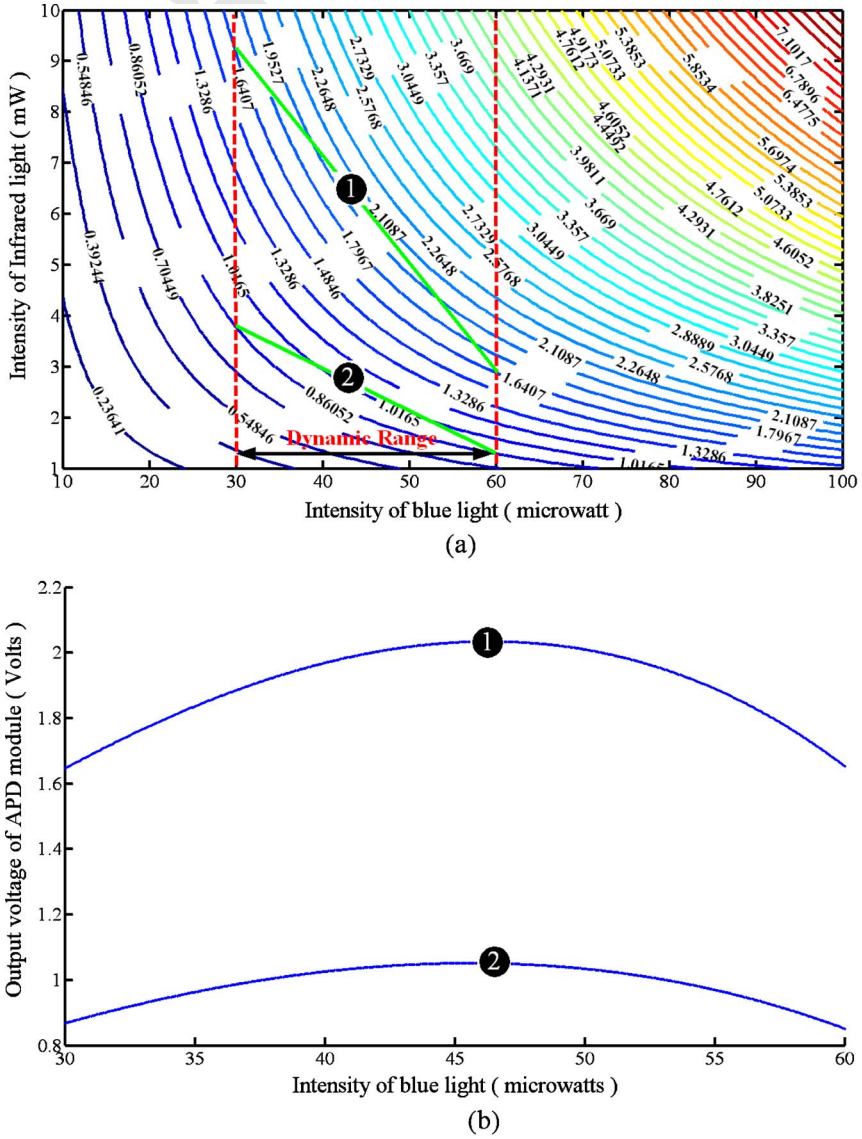

Color: Online

Fig. 13. (Color online) (a) Two LCLs with the same dynamic range. The termination points of each of these LCLs are located on the same contour. (b) The intensities of the emitted orange light along two LCLs that are depicted in Fig. 14(a).

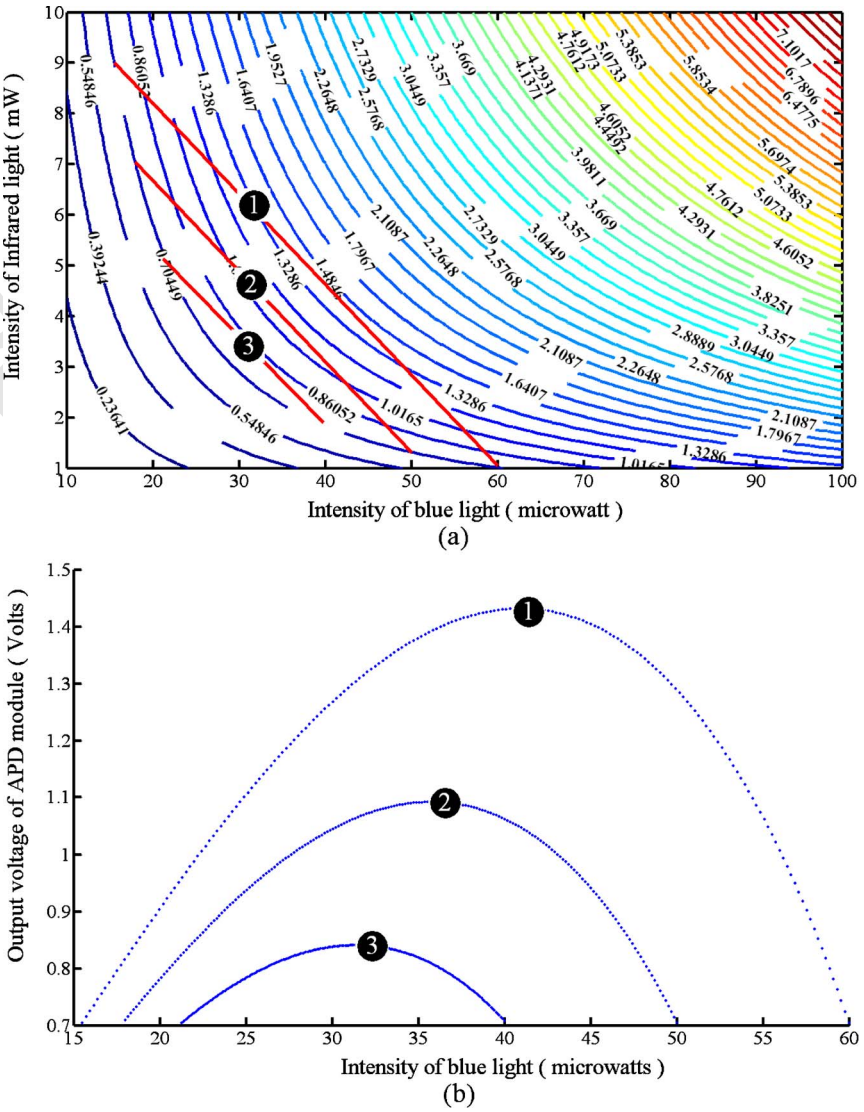

Color: Online

Fig. 14. (Color online) (a) Parallel LCLs. All the terminating points are on the same contour. (b) The crresponding nonlinear curves. This type of nonlinear curve can be used in the optical generation of one-dimensional maps.

$$\frac{\eta}{t+t_s}=\exp\left(\frac{n_s-n}{\xi I_{\mathrm{B}}}\right)-1. \tag{5}$$

Similarly, using Eq. (2), the reduction rate of the trapped-electron density during the discharging process is

$$\dot{n}=\frac{\mathrm{d}n}{\mathrm{d}t}=\frac{\xi' I_{\mathrm{NIR}}}{\eta'}\frac{\left[\exp\left(\frac{n}{\xi' I_{\mathrm{NIR}}}\right)-1\right]^2}{\exp\left(\frac{n}{\xi' I_{\mathrm{NIR}}}\right)}, \tag{6}$$

and by rearranging Eq. (2),

$$\frac{\eta'}{t+t_s'}=\exp\left(\frac{n}{\xi' I_{\mathrm{NIR}}}\right)-1. \tag{7}$$

Equations (5) and (7) can be solved for the parameters t_s and $t_{s'}$:

$$t_s=\frac{\eta}{\exp\left(\frac{n_s-n}{\xi I_{\mathrm{B}}}\right)-1}, \tag{8}$$

$$t_{s'}=\frac{\eta'}{\exp\left(\frac{n}{\xi' I_{\mathrm{NIR}}}\right)-1}. \tag{9}$$

Now, Eqs. (4) and (6) can also be rewritten in the forms

$$\dot{n}=\frac{4\xi}{\eta}I_{\mathrm{B}}\sinh^2\left(\frac{n_s-n}{2\xi I_{\mathrm{B}}}\right), \tag{10}$$

$$\dot{n}=-\frac{4\xi'}{\eta'}I_{\mathrm{NIR}}\sinh^2\left(\frac{n}{2\xi' I_{\mathrm{NIR}}}\right). \tag{11}$$

The mathematical model for the charging and discharging processes is expressed in Eqs. (10) and (11). By com-

bining these two expressions, we develop the mathematical model that governs the dynamics of the ETM under simultaneous blue light and NIR illumination:

$$\dot{n} = \frac{4\xi}{\eta} I_{\mathrm{B}} \sinh^2\left(\frac{n_s - n}{2\xi I_{\mathrm{B}}}\right) - \frac{4\xi'}{\eta'} I_{\mathrm{NIR}} \sinh^2\left(\frac{n}{2\xi' I_{\mathrm{NIR}}}\right). \tag{12}$$

Equation (12) provides a complete mathematical model for the dynamics of ETM in the form of a nonlinear differential equation.

Section 5 below is dedicated to the study of the equilibrium-state luminescence of ETM, which is the equilibrium state of Eq. (12) ($\mathrm{d}n/\mathrm{d}t = 0$):

$$\frac{4\xi}{\eta} I_{\mathrm{B}} \sinh^2\left(\frac{n_s - n^*}{2\xi I_{\mathrm{B}}}\right) = \frac{4\xi'}{\eta'} I_{\mathrm{NIR}} \sinh^2\left(\frac{n^*}{2\xi' I_{\mathrm{NIR}}}\right), \tag{13}$$

$$I_{\mathrm{O}}^* = \alpha n^* I_{\mathrm{B}} + \beta n^* I_{\mathrm{NIR}}. \tag{14}$$

In these equations, n^* and I_{O}^* are the trapped-electron density and the intensity of the orange luminescence in the equilibrium state, respectively. For any specified values of the blue light and NIR light intensities, Eq. (13) can be solved for n^* by minimizing the error function $\mathrm{er}f(n^*)$:

$$\mathrm{er}f(n^*) = \left\| \frac{4\xi}{\eta} I_{\mathrm{B}} \sinh^2\left(\frac{n_s - n^*}{2\xi I_{\mathrm{B}}}\right) - \frac{4\xi'}{\eta'} I_{\mathrm{NIR}} \sinh^2\left(\frac{n^*}{2\xi' I_{\mathrm{NIR}}}\right) \right\|. \tag{15}$$

In this equation, $\| \|$ is the Euclidean norm. If one has the value of n^*, the intensity of the orange light emission I_{O}^* is computable from Eq. (14). By this methodology, one can compute the value of I_{O} for a wide range of values of I_{B} and I_{NIR} and prepare a diagram like the one shown in Fig. 10. In this two-dimensional diagram, which is called the equilibrium-state plane (ESP) of the ETM, the contours of constant orange light emission intensity are plotted as a function of the blue light and NIR light intensity for a reasonable range of variables on each axis. The numbers on the contours are the output voltages of the photodetec-

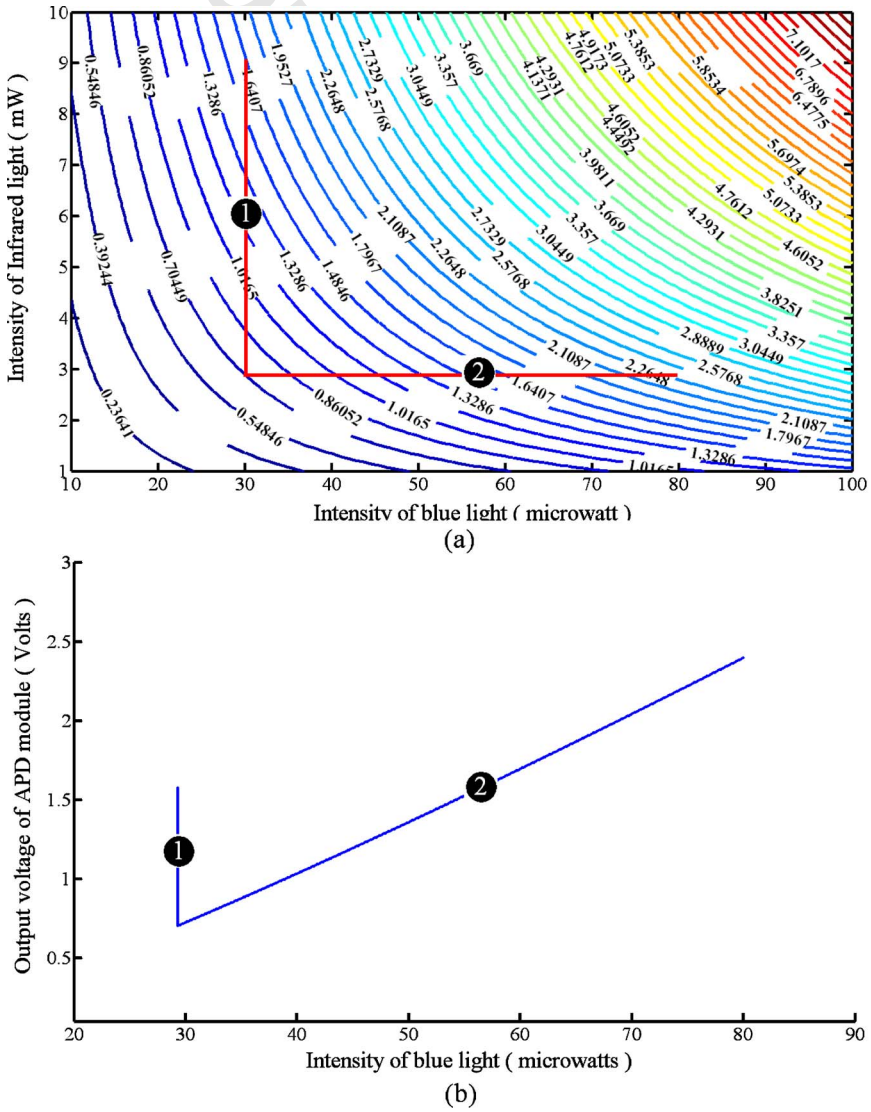

Color: Online

Fig. 15. (Color online) (a) Two LCLs for the generation of the quasi-linear curves. (b) The corresponding quasi-linear curves.

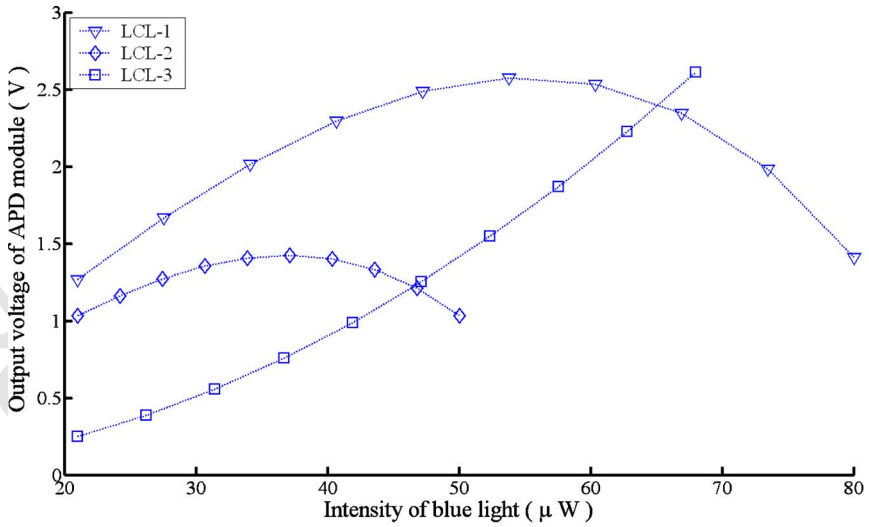

Color: Online

Fig. 16. (Color online) Experimental results. Along the first two LCLs, which have negative slopes, (see text) the luminescence of the material changes nonlinearly. Along the third LCL, which has positive slope, the luminescence of the material is quasi-linear.

tor that measures the intensity of the orange luminescence. In Section 5, we will use this diagram as a graphic tool to design highly nonlinear optical devices.

5. EQUILIBRIUM-STATE LUMINESCENCE

The significance of the equilibrium-state luminescence of ETM for applications in optical signal processing becomes clear by an example. Consider the simple optical arrangement displayed in Fig. 11(a). A photodetector measures the intensity of the light emitted from a light source and passed through a passive optical device. Usually, the output voltage of the photodetector is a linear function of the intensity of illumination. However, in many applications (e.g., optical realization of one-dimensional maps in nonlinear dynamics) we require a nonlinear behavior such as the desired curve depicted in Fig. 11(b). Here, the intensity of the detected light increases at first and decreases when we pass a maximum point. To our knowledge such an optical component is not available. In this section we show that the equilibrium-state luminescence of ETM can be controlled to exhibit such a nonlinear behavior. Based on the experimental results and the developed mathematical model, we then present an improved approach for realization and design of such nonlinear optical devices.

The behavior of ETM in the equilibrium state can be predicted by using the ESP diagram that was introduced in Section 4. We highlight the subtle utility of the ESP diagram by investigating four sample points, S, 1, 2, and 3, in Fig. 10. Point S corresponds to the ETM panel being exposed simultaneously to blue and NIR light with the ETM in the equilibrium state. The intensity of the incident blue light and the NIR exposure are 50 μW and 4.35 mW, respectively. The output voltage of the photodetector that measures the intensity of the orange light luminescence is $\approx$1.8 V.

Now, consider the case when the intensity of the blue light is increased from 50 μW to 60 μW, and in three succeeding steps, the intensity of the NIR light is changed to

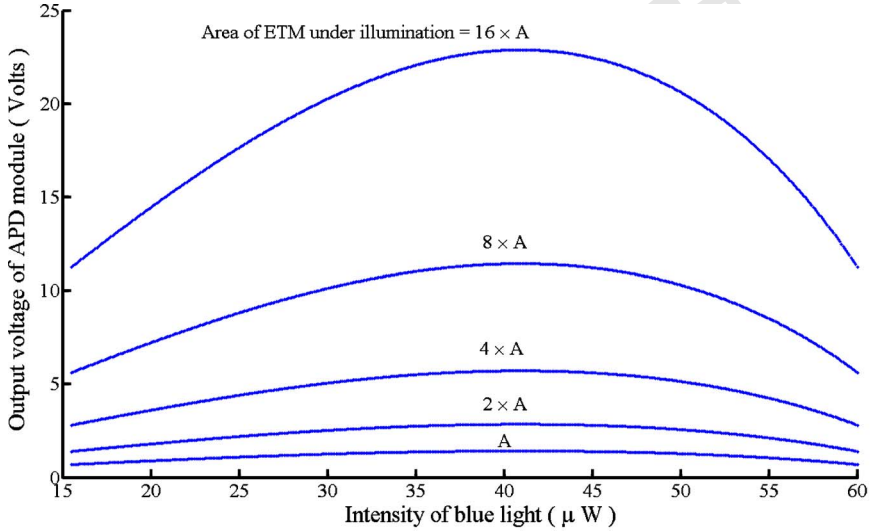

Color: Online

Fig. 17. (Color online) Effect of changing the area of the ETM under illumination. The nonlinear curves are related to the third LCL in Fig. 13(a). The area changes from $A=3$ mm^2 to $16\times A$.

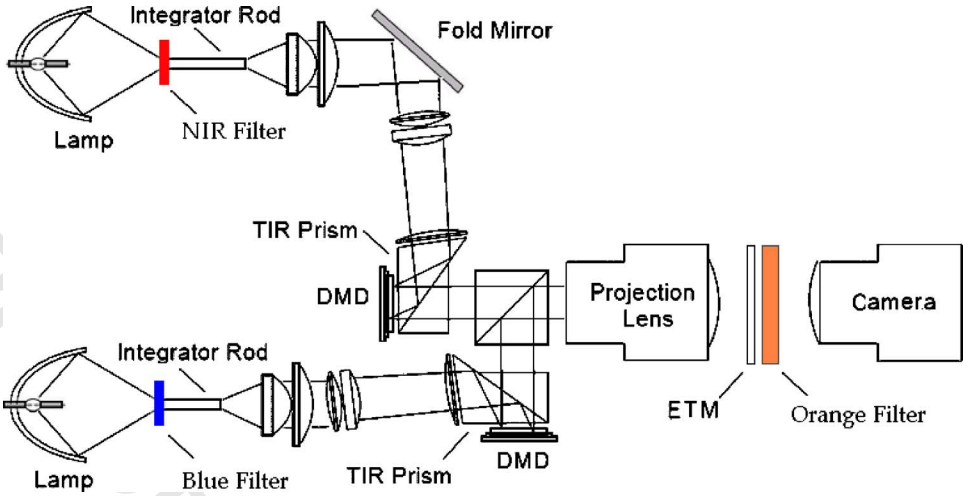

Color: Online

Fig. 18. (Color online) Simultaneous illumination of ETM panel with the combined beam of two DMD spatial light modulators. (TIR stands for total internal reflection.)

4 mW, 3.2 mW, and 2.6 mW. These new states are the points 1, 2, and 3, respectively, in Fig. 10. The output voltages of the photodetector at these three points are 2.1, 1.8, and 1.5 V for points 1, 2, and 3, respectively. As a result, by increasing the intensity of the blue light from point S to points 1, 2, and 3, depending on the intensity of the NIR illumination, the intensity of the orange luminescence increases, remains the same, or decreases, respectively. Further investigation reveals that the intensity of the emitted orange light monotonically increases along the line $S \rightarrow 1$ and decreases along the line $S \rightarrow 3$. We have recently shown that this kind of behavior can be used to model the excitatory and inhibitory responses of the neurons in optical realization of bio-inspired artificial neural networks [18,19].

Now consider the special case where the blue and NIR light sources are linearly coupled. The linear coupling of two light sources can be formulated by the equation

$$\mu I_{\mathrm{B}} + \nu I_{\mathrm{NIR}} = \sigma, \tag{16}$$

where μ, ν, and σ are real numbers. These variables are the key parameters in the design of the nonlinear optical device. In this paper, the line expressed by Eq. (16) is called the linear-coupling line (LCL). In the particular case where the light sources are coupled linearly, the optical device user can change the intensity of only one of the light sources. For instance, in this paper, the blue light source is the master source, and the NIR light source traces the blue light source through Eq. (16). When the two light sources are linearly coupled, those orange light emission intensities along the corresponding LCL only are achievable.

Two sample LCLs and their dynamic ranges over the horizontal axis are illustrated in Fig. 12(a). The intensity of the emitted orange light changes nonlinearly along these two lines as shown in Fig. 12(b). A variety of nonlinear curves are achievable by changing the slope and the location of a LCL in the ESP. For instance, the termination points of the first LCL in Fig. 12(a) are located on the two different constant voltage contours. Therefore, the intensities of the emitted orange light are different at these points. The second LCL has a different slope and dynamic range, and the corresponding nonlinear curve is quite different from the nonlinear curve of the first LCL; however, the termination points are both on the same contour. Therefore, the corresponding nonlinear orange light emission curve has equal intensities at the terminating points and the nonlinear curve is more symmetric.

These types of LCLs are suitable for the optical generation of nonlinear one-dimensional maps. Figure 13(a) displays two different LCLs with the same dynamic range. The corresponding nonlinear curves are illustrated in Fig. 13(b). In spite of similar dynamic ranges, these LCLs have different slopes and termination points. Hence, the corresponding nonlinear curves are different. A subtle difference between these two nonlinear curves is the speed of computation on these two LCLs. It should be remembered that all these curves are achievable in the equilibrium state of the ETM, which means that each time the intensities of the blue light and the NIR light are set, the user should wait for the equilibrium state to occur. The equilibrium is reached sooner for higher intensities of the blue and NIR light and larger density of the trapped electrons. The ETM reaches the equilibrium state faster along the second LCL of Fig. 13(a) than along the first LCL. Meanwhile, the intensity of orange luminescence is higher along the first LCL compared with the second one and the detected signal has a larger signal-to-noise ratio.

Now consider the case depicted in Fig. 14(a). In this figure, three parallel LCLs are shown in the ESP of the ETM. The corresponding orange light emission curves along these LCLs are shown in Fig. 14(b). The termination points of these three LCLs are placed on the same contour that represents the photodetector output voltage of $\approx$700 mV. These three LCLs are parallel to each other. Therefore, the parameters μ and ν in Eq. (16) are fixed, and the parameter σ is the only variable. In nonlinear-dynamic applications, σ can play the role of the bifurcation parameter. By normalizing the dynamic ranges of these lines, the developed nonlinear curves will look like the curves that are used in the generation of a one-dimensional map such as the logistic map in [20]. We should mention that the quasi-linear behavior can also be

generated by the equilibrium state of the ETM when the LCLs are chosen appropriately. Figs. 15(a) and 15(b) illustrate two LCLs and the corresponding quasi-linear functions, respectively.

In order to verify the above formulations an experiment was carried out using the optical setup of Fig. 2. We chose the following LCLs and measured the intensity of the orange luminescence in the equilibrium state along each line:

$$\text{LCL-1:} \quad -0.14I_B + I_{NIR} = 12.0,$$

$$\text{LCL-2:} \quad -0.18I_B + I_{NIR} = 11.0,$$

$$\text{LCL-3:} \quad +0.05I_B + I_{NIR} = 0.0.$$

The results are shown in Fig. 16. In all these experiments, the surface of the ETM panel is covered by a dark optical mask with a small aperture. Thus, the area of the ETM under illumination is fixed. On the other hand, one can effectively take advantage of the area as a parameter in the design of the nonlinear optical device. For a constant blue and NIR light illumination, the level of the orange light emission changes linearly as a function of the area of the ETM under illumination. Figure 17 shows the nonlinear curves developed by changing the illuminating area for the third LCL in Fig. 14(a). We can use these curves for the optical production of the one-dimensional maps without any normalization.

One can easily change the area of ETM under illumination by using a spatial light modulator such as the Texas Instruments digital micromirror device (DMD) [21]. A sample optical setup is depicted in Fig. 18. A DMD chip is a two-dimensional array of bistable programmable micromirrors. Two DMD modules in the setup provide the blue light and the NIR illuminations by reflecting the beam of two powerful light sources. By changing the number of mirrors, whose reflections expose the surface of the ETM, the illuminating area can be changed. DMDs are fast enough to adjust the area every few milliseconds, which is shorter than the few hundred milliseconds required for an ETM to reach the equilibrium state.

6. CONCLUSION

We have introduced an improved mathematical model that governs the dynamics of ETMs under blue light and near-infrared illumination. The model describes the evolution of an ETM's luminescence during charging, discharging, simultaneous illumination, and in the equilibrium state. This model, which is established based on the experimental results and takes into account some of the previously neglected effects, can improve the applicability of the ETM's unique dynamics, particularly in quantitative applications such as optical signal processing. We have also studied the nonlinear response of ETMs in the equilibrium state. This nonlinear response has potential applications in nonlinear optical signal processing and optical implementation of one-dimensional maps. There are occasions where collective processing in multiple one-dimensional maps needs to be considered. An obvious example of these applications are networks of one-dimensional maps [22–24]. The parallel computation carried out by such networks can be realized in a thin film of this storage phosphor addressed suitably employing DMD technology. Consequently, our mathematical model would be an important tool for effective use of an ETM's dynamics.

ACKNOWLEDGMENTS

This research was supported in part by Army Research Office Multidisciplinary University Research Initiative grant prime DAAD 19-01-0603 via Georgia Institute of Technology subcontract E-18-677-64 and in part by Office of Naval Research grant N00014-94-1-0931.

REFERENCES AND NOTES

1. J. Lindmayer, "A new erasable optical memory," Solid State Technol. **31**, 135–138 (1988).
2. J. Lindmayer, P. Goldmith, and K. Gross, "Electron-trapping optical technology—memory's next generation," Comput. Technol. Rev. **10**, 37–42 (1990).
3. S. Jutamuli, G. Stori, J. Lindmayer, and W. Seiderman, "Use of electron trapping materials in optical signal processing. 1: parallel Boolean logic," Appl. Opt. **29**, 4806–4811 (1990).
4. A. D. McAulay, J. Wang, and C. T. Ma, "Optical dynamic matched filtering with electron trapping devices," in *Real-Time Signal Processing XI*, J. P. Letellier, ed., Proc. SPIE 977, 271–276 (1988).
5. S. Jutamuli, G. Stori, J. Lindmayer, and W. Seiderman, "Use of electron trapping materials in optical signal processing. 2: two-dimensional associative memory," Appl. Opt. **30**, 2879–2884 (1991).
6. S. Jutamuli, G. Stori, J. Lindmayer, and W. Seiderman, "Use of electron trapping materials in optical signal processing. 3: modified Hopfield type neural networks," Appl. Opt. **30**, 1786–1790 (1991).
7. A. D. McAulay, J. Wang, and C. T. Ma, "Optical orthogonal neural network associative memory with luminescence rebroadcasting devices," in *Proceedings of the IEEE International Conference on Neural Networks* (Proc. IEEE 1989) pp. 483–485.
8. F. Itoh, K. Kitayama, and Y. Tamura, "Optical outer-product learning in a neural network using optically stimulable phosphor," Opt. Lett. **15**, 860–862 (1990).
9. S. Jutamulia, G. Storti, J. Lindmayer, and W. Seiderman, "Optical information processing systems and architectures," Proc. SPIE **1151**, 83–xx (1990).
10. P. Soltani, D. Brower, and G. Storti, "Electron image tubes and image intensifiers," Proc. SPIE **1243**, 114–xxx (1990).
11. S. Keller, J. Mapes, and G. Cheroff, "Studies on some infrared stimulable phosphors," Phys. Rev. **108**, 663–676 (1957).
12. Z. Wen and N. Farhat, "Dynamics of electron trapping materials for use in optoelectronic neurocomputing," Appl. Opt. **32**, 7251–7265 (1993).
13. Z. Wen, N. Farhat, "Electron trapping materials and electron-beam-addressed electron trapping material material devices: an improved model," Appl. Opt. **34**, 5188–5198 (1995).
14. X. Yang, C. Y. Wrigley, and J. Lindmayer, "Three-dimensional optical memory based on transparent electron thin film," Proc. SPIE **1773**, 413–422 (1992).
15. The electron-trapping material used for this investigation was furnished by the former Quantex Corporation, Rockville, Maryland, USA.
16. Z. Hua, L. Salamanca-Riba, M. Wuttig, and P. K. Soltani, "Temperature dependence of photoluminescence in $SrS:Eu^{2+},Sm^{3+}$ thin films," J. Opt. Soc. Am. B **10**, 1464–1469 (1993).
17. S. Boyd and L. Vandenberghe, *Convex Optimization*,

AQ: #4

available online at http://www.stanford.edu/boyd/cvxbook.html (Cambridge U. Press, 2004).

18. R. Pashaie and N. H. Farhat, "Optical realization of the retinal ganglion receptive fields in electron-trapping material thin film," Proceedings of 32nd Northeast Bioengineering Conference, Easton, Penn., USA (2006).

AQ: #5

19. R. Pashaie and N. H. Farhat, "Realization of receptive fields with excitatory and inhibitory responses on the equilibrium-state luminescence of electron trapping material thin film," Opt. Lett. (to be published).

20. S. H. Strogatz, *Nonlinear Dynamics and Chaos: With Applications to Physics, Biology, Chemistry and Engineering* (Da Capo Press, 1994).

21. D. Dudley, W. M. Duncan, and J. Slaughter, "Emerging digital micromirror device (DMD) applications," Proc. SPIE **4985**, 14–25 (2003).

22. K. Kaneko, "Overview of coupled map lattices," Chaos **2**, pp. 279–282 (1992).

23. N. H. Farhat, "Corticonics: the way to designing machines with brain-like intelligence," Proc. SPIE **4109**, 103–109 (2000).

24. N. H. Farhat, "Corticonic networks for higher-level processing," Proc. 2nd IASTED, Feb. 23–25 (2004), pp. 256–262.

AQ: #6

AUTHOR QUERIES — 545708JOB

#1 Au: Claims of “new” deleted for legal reasons.
#2 Au: Please define “lp” in “lp/mm”
#3 Au: Check math in Eq. (4). Are parens and brackets as meant? Also in following equations?
#4 Au: Please provide ending page number Refs. 9 and 10
#5 Au: Please provide full dates of conference OR name of publishor of proceedings for Ref. 18.
#6 Au: Ref. 24: Please provide full name of conference; spell out IASTED; give year of conf. and location.
#7 Au: Fig. 10 caption: Is “unexpected” as meant?